Applied Catalysis B: Environmental 97 (2010) 389–397

Contents lists available at ScienceDirect

Applied Catalysis B: Environmental

journal homepage: www.elsevier.com/locate/apcatb

Au-decorated $Na_xH_{2-x}Ti_3O_7$ nanobelts exhibiting remarkable photocatalytic properties under visible-light illumination

Ying-Chih Pu, Yu-Chih Chen, Yung-Jung Hsu*

Department of Materials Science and Engineering, National Chiao Tung University, 1001 University Road, Hsinchu 30010, Taiwan, ROC

ARTICLE INFO

Article history:
Received 18 February 2010
Received in revised form 21 April 2010
Accepted 23 April 2010
Available online 17 May 2010

Keywords:
Titanate
Nanobelts
Photocatalysis
Visible-light-driven
Charge separation

ABSTRACT

We demonstrated for the first time that Na-intercalated $H_2Ti_3O_7$ ($Na_xH_{2-x}Ti_3O_7$) NBs, prepared in the typical alkaline hydrothermal process, can effectively absorb visible light to carry out photocatalytic reactions. With the capability of effective light absorption in visible range, $Na_xH_{2-x}Ti_3O_7$ NBs performed much better in the photodegradation of thionine than the other three counterpart products including $H_2Ti_3O_7$, mixed $Na_2Ti_6O_{13}/TiO_2$ and anatase TiO_2 under visible-light irradiations. As compared to the relevant commercial products like P-25 TiO_2 and $Na_2Ti_3O_7$ powders, the as-synthesized $Na_xH_{2-x}Ti_3O_7$ NBs exhibited superior photocatalytic efficiency under UV illumination, demonstrating their potential as an efficient photocatalyst in relevant redox reactions. A further enhancement in the photocatalytic activity can be achieved for $Na_xH_{2-x}Ti_3O_7$ NBs when Au nanoparticles of suitable amount were deposited on their surfaces. This improvement is due to the band offsets between $Na_xH_{2-x}Ti_3O_7$ and Au, which may promote charge carrier separation to favor the photocatalysis. The recycling test reveals that Au-decorated $Na_xH_{2-x}Ti_3O_7$ NBs could be promisingly utilized in the long-term course of photocatalysis. Furthermore, the result of performance evaluation under natural sunlight shows that the current Au-decorated $Na_xH_{2-x}Ti_3O_7$ NBs can be used as highly efficient photocatalysts which may practically harvest energy from sunlight.

© 2010 Elsevier B.V. All rights reserved.

1. Introduction

With the concern about the environmental and energy issues, there has been a growing interest in developing semiconductor photocatalysts that can produce chemical energy from light [1,2]. The basic concept of photocatalysis using semiconductors involves the generation of charge carriers within semiconductors upon light irradiation, followed by the utilization of these carriers to carry out chemical reactions. In general, the fast recombination of photoexcited charge carriers in semiconductors would diminish the resulting photocatalytic efficiency. To boost photocatalytic performance, the photoexcited electrons and holes must be separated to suppress the direct recombination of them. Through the combination with metals, semiconductors may exhibit superior photocatalytic activities. This is due to the presence of semiconductor/metal interface that can promote charge carrier separation [3,4]. In semiconductor/metal heterostructures, metal can serve as an efficient electron scavenger for semiconductor. The photoexcited free electrons of semiconductor would thus preferentially transfer to the metal domain, leading to the effective separation of charge carriers to favor the subsequent photocatalysis. Till now, many hybrid systems composed of semiconductors and metals, such as core–shell metal–semiconductor nanocrystals [5,6], metal-decorated semiconductor nanorods [7,8], and metal-deposited semiconductor nanoparticles [9,10], have been proposed and characterized to demonstrate their remarkable performance in relevant photocatalytic processes.

The most widely used semiconductor photocatalysts have been metal oxides like TiO_2, which possesses ultraviolet (UV) absorption ability only because of its large bandgap energy. In order to practically harvest energy from sunlight, a lot of research attention is paid to manufacture photocatalysts that can respond to visible light. It has been extensively demonstrated that II–VI group semiconductors such as CdS [11,12] and CdSe [13,14] exhibit fascinating photocatalytic activities upon visible-light irradiation. The potential danger of cadmium to the organisms however limits the practical development for these cadmium derivative photocatalysts. On the other hand, through the doping of suitable elements to create an additional electronic level in the energy gap, TiO_2 can absorb visible light to carry out photocatalytic reactions [15–17]. The introduction of foreign elements into TiO_2 crystals was usually accomplished under elaborate reaction conditions, for example, high reaction temperatures [18,19] and long period of treatment in harsh atmospheres [20,21]. Such requirement complicates the configuration of manufacture process and considerably raises the cost for scale-up production. Moreover, a depressed carrier mobil-

* Corresponding author. Tel.: +886 3 5712121x55317; fax: +886 3 5724724.
E-mail address: yhsu@cc.nctu.edu.tw (Y.-J. Hsu).

0926-3373/$ – see front matter © 2010 Elsevier B.V. All rights reserved.
doi:10.1016/j.apcatb.2010.04.023

ity as well as the low quantum yield were observed for the doped TiO_2 under visible-light illumination [22,23], which may further hinder its performance in photocatalysis. Therefore, creation of a more facile, mild synthetic approach from which one could obtain highly efficient visible-light-responsive photocatalysts is crucial to the development of photocatalysis technology.

Nanostructures of sodium titanate ($Na_2Ti_nO_{2n+1}$, $3 \leq n \leq 6$) and hydrogen titanate ($H_2Ti_nO_{2n+1}$) have draw much research attention in recent years due to their unique physicochemical and chemical properties [24], which open up potential applications in photocatalysis [25,26], chemical adsorption [27,28], hydrogen storage [29,30], lithium batteries [31,32], and biomedics [33,34]. Since the pioneering work by Kasuga et al. [35,36], alkaline hydrothermal approach has been widely employed to produce these Ti–O based nanostructures. Through carefully controlling the hydrothermal conditions, various nanostructures of titanates including nanoparticles, nanotubes, and nanobelts can be readily obtained in high yield [37]. As one of the Ti–O series products derived from the alkaline hydrothermal process, Na-intercalated $H_2Ti_3O_7$ ($Na_xH_{2-x}Ti_3O_7$) [38–41] does not draw too much research attention, especially in the field of photocatalysis. This is probably due to the ion-exchangeability of $Na_xH_{2-x}Ti_3O_7$, which enables feasible compositional transformation into its protonated form of $H_2Ti_3O_7$.

In this work, we demonstrated for the first time that $Na_xH_{2-x}Ti_3O_7$ nanobelts (NBs) can effectively absorb visible light to carry out photocatalytic reactions. NBs of $Na_xH_{2-x}Ti_3O_7$ were synthesized in a typical alkaline hydrothermal reaction by using P-25 TiO_2 powder as precursor [37]. This synthetic route is simple, reliable and can be easily scaled-up to achieve mass production. In addition to $Na_xH_{2-x}Ti_3O_7$ NBs, three other Ti–O counterpart products including hydrogen titanate ($H_2Ti_3O_7$), mixed sodium titanate/titania ($Na_2Ti_6O_{13}/TiO_2$), and single-phase anatase titania (TiO_2) were also prepared by a proper post-treatment operation. We evaluated and compared the photocatalytic performance of the four Ti–O based samples through the photodegradation of an organic dye, thionine (TH). With the capability of effective light absorption in visible range, $Na_xH_{2-x}Ti_3O_7$ NBs performed much better in the photodegradation of TH than the other three counterparts under visible-light irradiations. As compared to the relevant commercial products like P-25 TiO_2 and $Na_2Ti_3O_7$ powders, the as-synthesized $Na_xH_{2-x}Ti_3O_7$ NBs exhibited superior photocatalytic performance under UV illumination, demonstrating their potential as an efficient photocatalyst in relevant redox reactions. A further enhancement in the photocatalytic activity can be achieved for $Na_xH_{2-x}Ti_3O_7$ NBs with the decoration of Au nanoparticles. Moreover, no appreciable decay of photocatalytic efficiency was found for Au-decorated $Na_xH_{2-x}Ti_3O_7$ NBs after repeated uses and recycled, revealing their promising potential in the long-term course of photocatalysis. The photocatalytic performance under natural sunlight was also examined, and the result shows that the current Au-decorated $Na_xH_{2-x}Ti_3O_7$ NBs can be used as highly efficient photocatalysts which may practically harvest energy from sunlight.

2. Experimental

2.1. Chemicals

All chemicals were of analytic grade and used without further purification.

2.2. Preparation of $Na_xH_{2-x}Ti_3O_7$ NBs

$Na_xH_{2-x}Ti_3O_7$ NBs were synthesized with a hydrothermal method in the concentrated NaOH solution. Typically, commercial TiO_2 powder of 1.0 g (Degussa, P-25) was dispersed in 10 mL absolute ethanol, and then mixed with 10 mL NaOH aqueous solution (10 M) under vigorous stirring for 10 min. The mixed solution was transferred into a Teflon-lined stainless-steel autoclave with a capacity of 100 mL. After being sealed, the autoclave was heated and maintained at 200 °C for 24 h, and then cooled to room temperature naturally. The resultant white slurry was collected by suction filtration and washed with deionized water until the pH value of washing solution reached 7.0. The product ($Na_xH_{2-x}Ti_3O_7$ NBs) was then dried at 60 °C in air for later use.

2.3. Acid-washing treatment

$Na_xH_{2-x}Ti_3O_7$ NBs of 0.3 g were immersed in 500 mL HCl solution (0.1 M) for 24 h, producing their protonated form of $H_2Ti_3O_7$. The product ($H_2Ti_3O_7$ NBs) was washed with copious amounts of deionized water and dried at 60 °C in air for later use.

2.4. Thermal calcination treatment

To prepare single-phase anatase TiO_2 NBs, $H_2Ti_3O_7$ NBs of a fixed amount were calcinated at 700 °C in air for 4 h. For comparison purpose, $Na_xH_{2-x}Ti_3O_7$ NBs were also allowed for thermal calcination under the same conditions, which led to the formation of mixed $Na_2Ti_6O_{13}/TiO_2$ with irregular morphology.

2.5. Decoration of Au nanoparticles

To decorate NBs with Au nanoparticles, $Na_xH_{2-x}Ti_3O_7$ NBs of 6.0 mg were first dispersed in the reaction solution containing 60 mL deionized water and 30 mL ethanol, followed by the addition of 600 μL NaOH solution (0.1 M). After heated to 50 °C, 60 μL of $HAuCl_4$ solution (5 mM) was added. Note that ethanol was used as the reducing agent [42] to facilitate the growth of Au. The mixed solution was kept at 50 °C for 3 h, resulting in the deposition of Au nanoparticles on the surfaces of $Na_xH_{2-x}Ti_3O_7$ NBs. The product (Au-decorated $Na_xH_{2-x}Ti_3O_7$ NBs with the Au content of 1.0 wt%) was centrifuged, washed with deionized water and ethanol, and then dried at 60 °C in air for later use. In this work, various volumes of $HAuCl_4$ solution (5 mM) were employed to produce Au-decorated NBs with increasing Au contents. Besides, two other novel metals (Ag and Pt) were also deposited on NB surfaces, with which we may learn the effects of various metal decorations on the photocatalytic properties of $Na_xH_{2-x}Ti_3O_7$ NBs. For the synthesis of Ag-decorated $Na_xH_{2-x}Ti_3O_7$ NBs, $AgNO_3$ was used as the Ag source, followed by the same procedure performed in the preparation of Au-decorated sample. As to the fabrication of Pt-decorated $Na_xH_{2-x}Ti_3O_7$ NBs, H_2PtCl_6 was used as the Pt source, followed by the same procedure mentioned above except for the reaction temperature and reaction time set at 80 °C and 6 h, respectively.

2.6. Photocatalytic performance measurement

The photocatalytic performance of the four Ti–O based samples was evaluated by the photodegradation of thionine (denoted as TH) under both UV and visible-light irradiations. A quartz tube with a capacity of 20 mL was used as the photoreactor vessel. The optical system used for TH photodegradation consisted of a xenon lamp (500 W, 175 mW/cm^2) and a bandpass filter (bandwidth of 400–700 nm) which enabled irradiation in visible range. All the photocatalysis experiments were conducted at room temperature. In a typical experiment, 5.0 mg of photocatalyst was added into 20 mL of TH solution in the photoreactor vessel. The TH solution was prepared by dissolving thionine acetate ($C_{14}H_{13}N_3O_2S$) in deaerated ethanol with a concentration of 1.0×10^{-5} M. Note that ethanol was used as the sacrificial hole scavenger for photocatalysts to facilitate the further utilization of photoexcited electrons.

Prior to irradiation, the suspension was stirred in the dark for 10 min to reach the adsorption equilibrium of TH with photocatalysts. At certain time intervals of irradiation, 1.5 mL of the reaction solution was withdrawn and centrifuged to remove the photocatalyst particles. The filtrates were analyzed with a UV–visible spectrophotometer to measure the concentration variation of TH through recording the corresponding absorbance of the characteristic peak at 605 nm. To investigate the recyclability and stability of photocatalysts, five cycles of photocatalytic reactions were conducted by using Au-decorated $Na_xH_{2-x}Ti_3O_7$ NBs with the Au content of 1.0 wt% as the representative sample. In addition, photodegradation of TH (1.0×10^{-5} M) under natural sunlight by using Au-decorated $Na_xH_{2-x}Ti_3O_7$ NBs (5.0 mg) as photocatalyst was also examined.

2.7. Characterization

Scanning electron microscopy (SEM) images were taken on JEOL JSM-6700 operated at an accelerated voltage of 15 kV. Energy dispersive spectrometry (EDS) analysis was performed on the facility of JSM-6700 at an accelerated voltage of 15 kV. Transmission electron microscopy (TEM) and high-resolution transmission electron microscopy (HRTEM) images were obtained using a JEOL JEM-2010 electron microscope operated at 200 kV. Powder X-ray diffraction (XRD) patterns were obtained with a MAC Sience MXP18 diffractometer using Cu Kα radiation (λ = 1.5405 Å) at 45 kV and 40 mA. X-ray photoelectron spectroscopy (XPS) data were recorded with a VG Scientific Microlab 350 electron spectrometer using Mg Kα ($h\upsilon$ = 1253.6 eV) as X-ray source under a base pressure of 1.0×10^{-9} Torr. The spectrum resolution of XPS was 0.1 eV, and the pass energy for survey and fine scans was 40 eV. All the binding energies were calibrated by C 1s at 284.6 eV. The deconvolution of O 1s XPS spectra of samples was performed using XPSPEAK software with 20% Lorentzian and 80% Gaussian peak feature set for the fitting. UV–visible absorption spectra were recorded using a Hitachi U-3900H spectrophotometer at room temperature under ambient atmosphere. Brunauer–Emmett–Teller (BET) surface area of the samples was estimated from the N_2 adsorption/desorption analysis.

3. Results and discussion

3.1. Structural investigation

Fig. 1 shows the SEM images and XRD patterns of the four Ti–O based samples prepared in this work. First, $Na_xH_{2-x}Ti_3O_7$ NBs with a typical width of 30–70 nm and length up to a few μm were obtained with the alkaline hydrothermal method. The *x* value of $Na_xH_{2-x}Ti_3O_7$ was about 0.66 according to the SEM-EDS and XPS results. The corresponding XRD pattern can be indexed as the typical layered titanate structures which exhibit a characteristic diffraction peak at 2θ of 10° [38,39]. Upon an acid-washing treatment in HCl for 24 h, a complete ion-exchange of Na with H was achieved for $Na_xH_{2-x}Ti_3O_7$ NBs, which led to a compositional transformation into $H_2Ti_3O_7$. As shown in Fig. 2, both the SEM-EDS and XPS measurements reveal the disappearance of Na constituent for NBs after the acid-washing operation. In Fig. 2b, the O 1s XPS spectrum of $Na_xH_{2-x}Ti_3O_7$ NBs displays two chemical states: the O1 component at 529.7 eV, which was assigned to the bonded oxygen in lattice (Ti^{4+}–O), and the O2 component at 531.7 eV, corresponding to the surface-adsorbed hydroxides (Ti–OH) [41]. After the acid-washing process, the O2 peak grew significantly to dominate over O1. This is mainly a result of the successful ion-exchange with H atoms, which caused an increasing amount of surface hydroxides for NBs [43]. Additionally, the slight shrinkage of interlayer

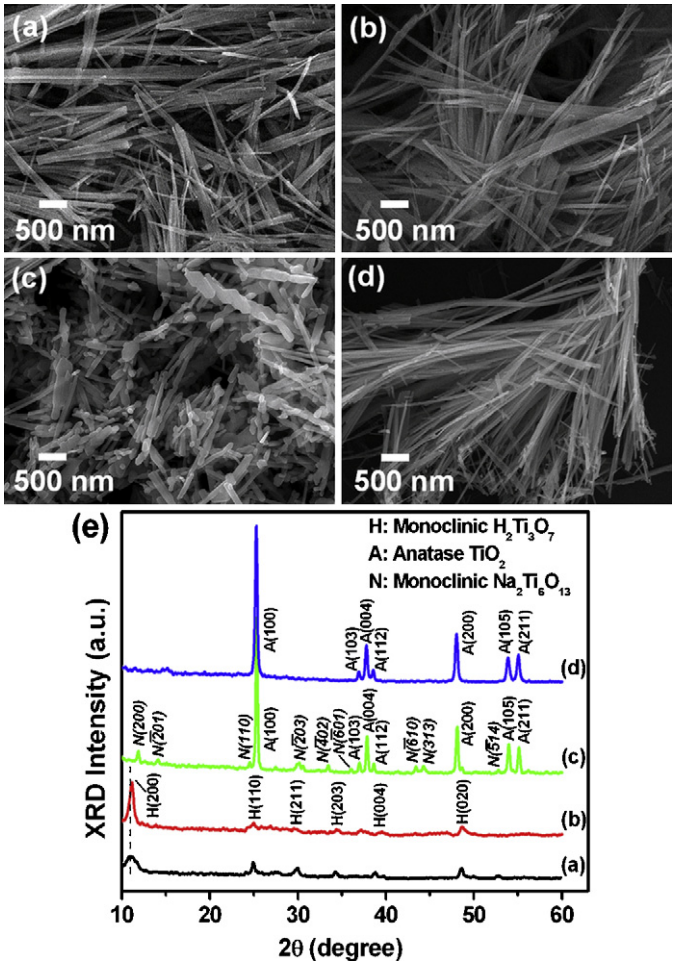

Fig. 1. SEM images of (a) $Na_xH_{2-x}Ti_3O_7$, (b) $H_2Ti_3O_7$, (c) calcinated $Na_xH_{2-x}Ti_3O_7$, and (d) calcinated $H_2Ti_3O_7$ samples. The corresponding XRD patterns were shown in (e).

spacing in the acid-treated sample, indicated by the slight shift of (2 0 0) diffraction peak toward higher 2θ, also confirms the replacement of Na with H atoms of smaller atomic size [40,44]. When $H_2Ti_3O_7$ was further calcinated at 700 °C in air for 4 h, single-phase anatase TiO_2 was produced through a dehydration process [45]. On the contrary, when $Na_xH_{2-x}Ti_3O_7$ sample was calcinated under the same conditions, a new phase of titanate, $Na_2Ti_6O_{13}$, formed along with the anatase TiO_2. It has been reported that upon a proper heat treatment, the $[Ti_3O_7]^{2-}$ layers of $Na_2Ti_3O_7$ crystals formed $[Ti_6O_{13}]^{2-}$ fragments that sheared vertices with each other via the topotactical connection [40]. The intercalating Na atoms were then accommodated within the interlayers of $[Ti_6O_{13}]^{2-}$ to result in the formation of $Na_2Ti_6O_{13}$. For the current $Na_xH_{2-x}Ti_3O_7$ NBs, the crystal lattice with intercalating Na principally underwent the topotactical connection process to form $Na_2Ti_6O_{13}$ upon the calcination treatment; meanwhile, the lattice containing H atoms was primarily dehydrated to produce TiO_2. A mixed phase of $Na_2Ti_6O_{13}$ and TiO_2 was consequently observed in the calcinated $Na_xH_{2-x}Ti_3O_7$ sample. Note that both $H_2Ti_3O_7$ and TiO_2 products preserved the NB morphology with similar dimensions to the as-prepared $Na_xH_{2-x}Ti_3O_7$ NBs. As regards the mixed $Na_2Ti_6O_{13}/TiO_2$ product, a large quantity of nanorods accompanied by a few granular particles was existent. The breakage of NB structures in the calcinated $Na_xH_{2-x}Ti_3O_7$ sample can be ascribed to the significant lattice distortion and lattice rearrangement that occurred during the intricate composition–conversion process from $Na_xH_{2-x}Ti_3O_7$ to $Na_2Ti_6O_{13}/TiO_2$.

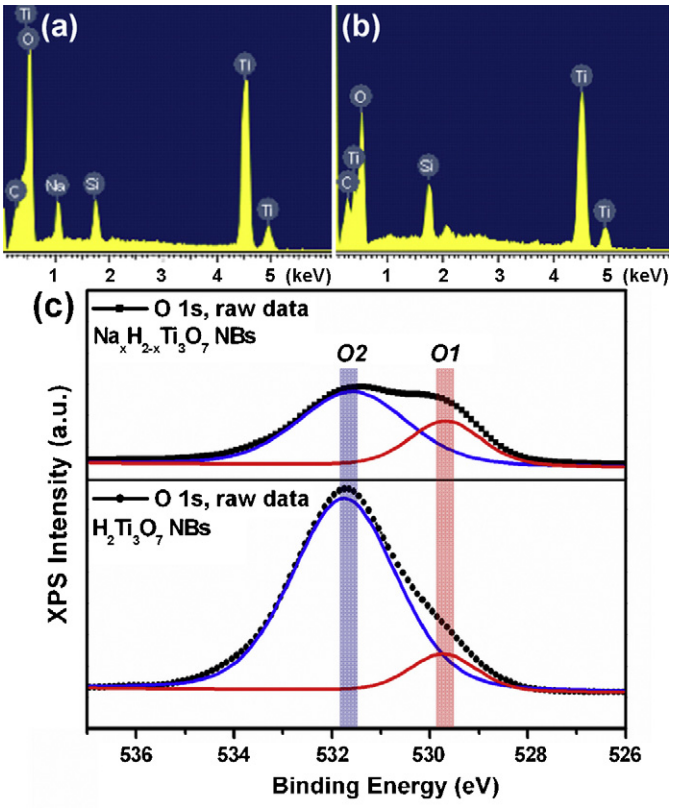

Fig. 2. SEM-EDS spectra of (a) $Na_xH_{2-x}Ti_3O_7$ and (b) $H_2Ti_3O_7$ NBs. The corresponding O 1s XPS spectra were shown in (c).

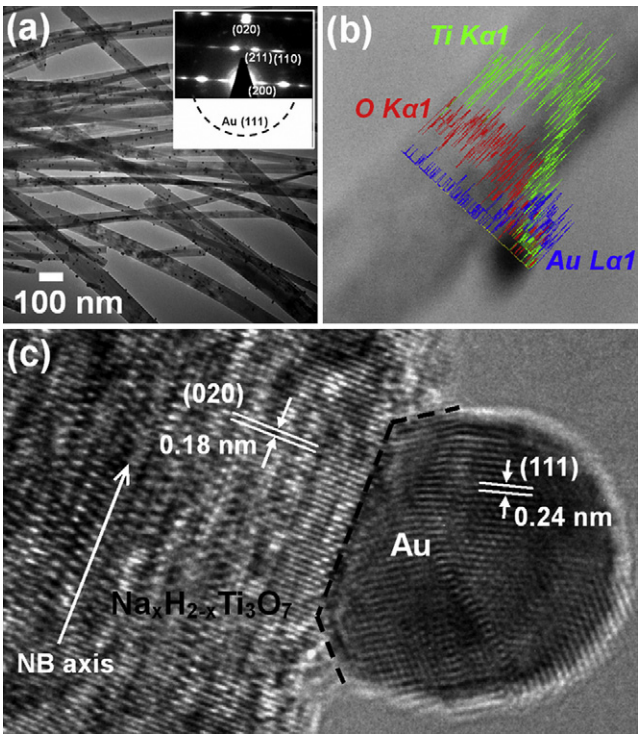

Fig. 3. (a) Typical TEM image of Au-decorated $Na_xH_{2-x}Ti_3O_7$ NBs with the ED patter shown in inset. (b) TEM-EDS elemental mapping and (c) HRTEM image taken on an individual Au-decorated $Na_xH_{2-x}Ti_3O_7$ NB. In (c), the interface of $Na_xH_{2-x}Ti_3O_7$/Au was highlighted with the dashed line. Content of Au = 10 wt%.

3.2. Decoration of Au nanoparticles

The decoration of Au nanoparticles on NBs was carried out with a chemical reduction approach. We chose $Na_xH_{2-x}Ti_3O_7$ NBs as the support for Au deposition, and the results were shown in Figs. 3 and 4. Fig. 3a represents the morphology of $Na_xH_{2-x}Ti_3O_7$ NBs after they were reacted with $HAuCl_4$ in the chemical reduction process. Evidently, a large quantity of nanoparticles with a size of 8–10 nm were present on the NB surfaces. The corresponding electron diffraction (ED) pattern, shown in the inset of Fig. 3a, implies the presence of Au, with the dot patterns contributed by the highly crystalline NBs and ring patterns by Au. The TEM-EDS line scan, shown in Fig. 3b, verifies that these nanoparticles were Au. Fig. 3c further shows the detailed crystallographic structures of the as-obtained Au-decorated $Na_xH_{2-x}Ti_3O_7$ NBs. In Fig. 3c, an HRTEM image taken at the interface of NB and nanoparticle regions clearly reveals two distinct sets of lattice fringes. An interlayer spacing of 0.18 nm was observed in the NB region, in good agreement with the *d* spacing of the (0 2 0) lattice planes of NBs, as determined from their corresponding XRD analysis in Fig. 1e ($d(0\,2\,0) = 0.187$ nm). In the particle region, an interlayer spacing of 0.24 nm was obtained, complying with the lattice spacing of (1 1 1) planes of the fcc Au [46]. This result, together with those of ED and TEM-EDS analyses, confirms the formation of Au nanoparticles on the surfaces of $Na_xH_{2-x}Ti_3O_7$ NBs upon the chemical reduction reaction.

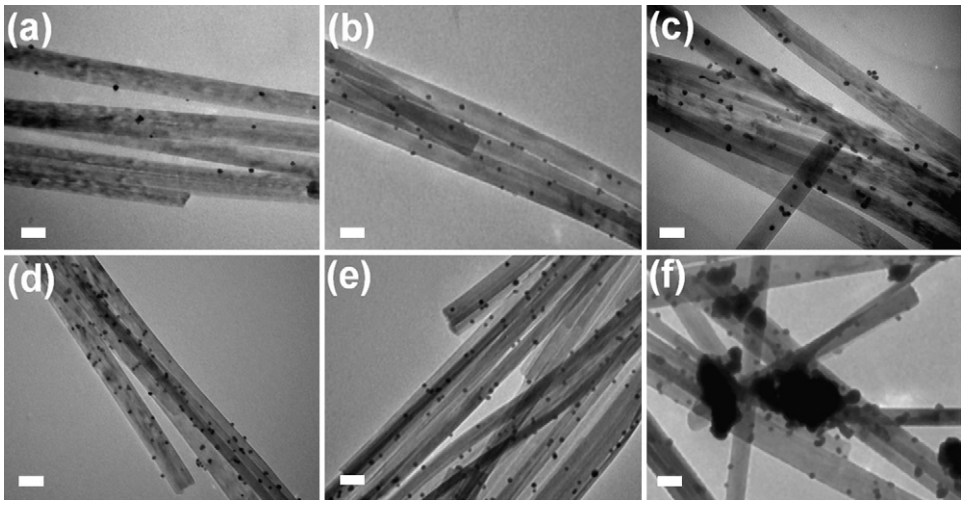

Fig. 4. TEM images of Au-decorated $Na_xH_{2-x}Ti_3O_7$ NBs with the Au contents of (a) 1.0, (b) 2.0, (c) 3.0, (d) 5.0, (e) 10 and (f) 50 wt%. Scale bar = 50 nm.

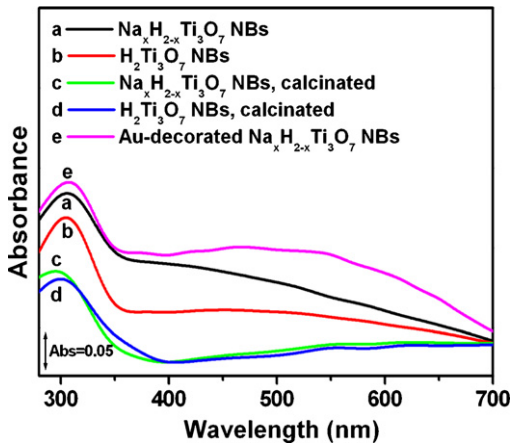

Fig. 5. UV–visible absorption spectra for the four Ti–O based samples. The spectrum of Au-decorated $Na_xH_{2-x}Ti_3O_7$ NBs with the Au content of 50 wt% was also included for comparison. Inserted arrow represents the scale of absorbance.

The success of this chemical reduction approach to decorate NBs with Au was achieved by utilizing NaOH as the complexing reagent. A plausible mechanism for the formation of Au-decorated $Na_xH_{2-x}Ti_3O_7$ NBs is proposed as follows. At the initial stage of reaction, $HAuCl_4$ was hydrolyzed to form Au chloro-hydroxyl complexes through the replacement of Cl^- with OH^- ligands which were provided by NaOH. Under the conditions of reaction (50 °C, 5 mM of $HAuCl_4$, and pH value of 11.2), the speciation of Au in solution was mainly $AuCl(OH)_3^-$ [47,48]. On the other hand, the surfaces of $Na_xH_{2-x}Ti_3O_7$ NBs were believed to adsorb numerous hydroxide species, as evident from the XPS analysis of Fig. 2c. A further complexation reaction between $AuCl(OH)_3^-$ and surface hydroxides of NBs can then proceed to lead to the attachment of Au complexes to NB surfaces (Ti–O–Au–Cl_2) [49]. During the reaction process, these Au complexes, predominately attached on the surfaces of NBs, decomposed to yield Au nuclei on NB surfaces. A crystallization stage subsequently ensued for Au to deposit onto these nucleation sites, resulting in the formation of Au-decorated $Na_xH_{2-x}Ti_3O_7$ NBs. By suitably controlling the experimental conditions such as the reaction temperature, the reaction time, and the amount of $HAuCl_4$, we were able to modulate the density of Au nanoparticles deposited on the surfaces of NBs. Fig. 4 reveals the gradual increase in Au particle density for Au-decorated $Na_xH_{2-x}Ti_3O_7$ NBs, which was achieved by employing $HAuCl_4$ of increasing amounts. Note that in a moderate range of $HAuCl_4$ amount, the as-grown Au nanoparticles were of similar size and distributed uniformly on the NB surfaces. As increasing the amount of $HAuCl_4$ to a relatively high value (for example, 50 wt% of Au content), bulky Au with irregular shape, apparently arising from the overgrowth of Au, became prevalent and stained on NB surfaces. It should be noted that Au-free NBs or free-standing Au nanoparticles were rarely observed in the products, demonstrating the advantage of the current approach to obtain Au-decorated NBs. Besides, the present chemical reduction approach can be extended to obtain other novel metal-decorated NBs such as Ag- and Pt-decorated samples, with which we may learn the effects of various metal decorations on the photocatalytic properties of $Na_xH_{2-x}Ti_3O_7$ NBs, as discussed later.

3.3. UV–visible absorption properties

The optical properties of the four Ti–O based samples were characterized with UV–visible spectroscopy. As displayed in Fig. 5, all the products showed strong light absorption in the range of 300–400 nm, which is characteristic of their corresponding excitonic bandgap absorption [50,51] (3.6 eV for $H_2Ti_3O_7$, 3.4 eV for $Na_2Ti_6O_{13}$, and 3.2 eV for anatase TiO_2). More importantly, an additional absorption band in visible range (400–700 nm) was observed for $Na_xH_{2-x}Ti_3O_7$ NBs. Such absorption band can be attributed to the intercalating Na atoms that may invoke interband transitions within the energy gap of NBs. Similar phenomena were ever reported for metal-intercalated $H_2Ti_3O_7$ nanotube systems [52], in which the introduced metals were supposed to induce extra electronic states in the forbidden gap through their delocalization and interaction with Ti 3d and O 2p orbitals. The metal-induced electronic states provided additional paths for exciton transition, thus resulting in the redshift of absorption band toward visible region. For the current $Na_xH_{2-x}Ti_3O_7$ NBs, new impurity levels might be created by the intercalating Na, from which electrons with lower energy can still transit to the conduction band. Accordingly, an obvious light absorption in visible range was observed. The effective light absorption in visible region may benefit the current $Na_xH_{2-x}Ti_3O_7$ NBs particularly in the photocatalysis aspect, since it adequately improved the efficiency of photon harvesting. Besides, $Na_xH_{2-x}Ti_3O_7$ NBs showed the most significant increase in light absorbance from 700 to 400 nm among the four Ti–O based products, which indicates that $Na_xH_{2-x}Ti_3O_7$ NBs were the only sample that may effectively absorb visible light to generate charge carriers. Also included in Fig. 5 was the spectrum of Au-decorated $Na_xH_{2-x}Ti_3O_7$ NBs. A much more evident light absorption in visible range was observed for Au-decorated $Na_xH_{2-x}Ti_3O_7$ NBs, probably resulting from the surface plasmon resonance effect exerted by Au nanoparticles [53]. This result reveals that Au-decorated $Na_xH_{2-x}Ti_3O_7$ NBs retained the capability of visible-light absorption for carrying out photocatalysis, as demonstrated later.

3.4. Photocatalytic properties

A series of photocatalysis experiments were performed in this work to investigate the photocatalytic properties of the four Ti–O based samples. TH, a cationic dye that can be decomposed by accepting electrons following the irradiation on photocatalysts, was used as the test pollutant [54]. The time-dependent UV–visible spectra of TH solutions under UV illumination in the presence of $Na_xH_{2-x}Ti_3O_7$ NBs were first shown in Fig. 6a. It can be seen that the intensity of the characteristic absorption peak at 605 nm decreased with the irradiation time. The bleaching of the absorption at 605 nm implies the reduction of TH to its leuco form [54], demonstrating the successful degradation of TH by using $Na_xH_{2-x}Ti_3O_7$ NBs as photocatalysts. To thoroughly understand the progress of TH photodegradation for our samples, we analyzed the normalized concentration of TH (C/C_o) as a function of irradiation time. Fig. 6b compares the photocatalytic performance among all the Ti–O based products under UV illumination. We noticed that experiment in the absence of photocatalyst showed slight degradation of TH, indicating a minor self-photolysis of TH molecules under UV illumination. After 120 min of irradiation, about 91% of TH was degraded by $Na_xH_{2-x}Ti_3O_7$ NB sample, whereas $H_2Ti_3O_7$, calcinated $Na_xH_{2-x}Ti_3O_7$ and calcinated $H_2Ti_3O_7$ samples only degraded 81, 71, and 82% of TH, respectively. We therefore concluded that $Na_xH_{2-x}Ti_3O_7$ NBs surpassed the other three counterpart products in the photocatalytic performance. The better photocatalytic efficiency observed in $Na_xH_{2-x}Ti_3O_7$ NBs can be accounted for by the intercalating Na atoms that induced extra electronic levels in the forbidden gap. Similar to the cases of doped TiO_2 [55,56], the Na-induced dopant levels in present NBs may act as either the donor or the acceptor centers to trap excitons, which further prohibited charge carriers from recombination. Therefore, $Na_xH_{2-x}Ti_3O_7$ NBs exhibited better photocatalytic efficiency than the other three undoped counterpart products under UV illumination. It might be argued that the surface area of NBs played

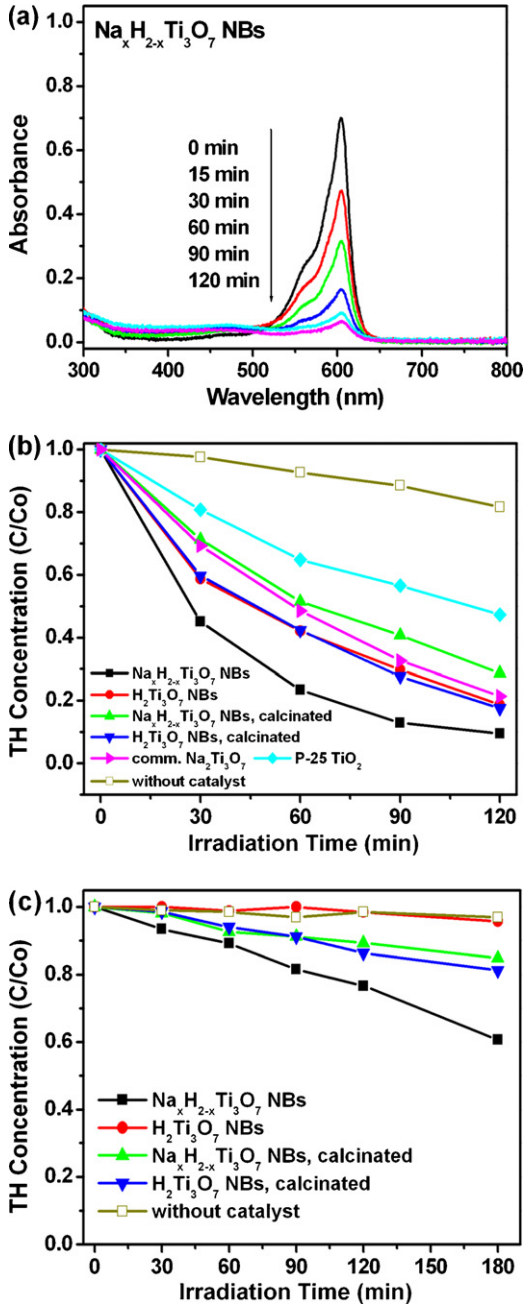

Fig. 6. (a) Absorption spectra of TH solutions under different UV irradiation times by using $Na_xH_{2-x}Ti_3O_7$ NBs. (b) C/C_0 versus irradiation time plots for TH photodegradation under UV illumination without any catalyst and in the presence of the four Ti–O based samples. The results by using commercial P-25 TiO_2 and $Na_2Ti_3O_7$ powders were also included for comparison. (c) C/C_0 versus irradiation time plots for TH photodegradation under visible-light irradiation by using the four Ti–O based samples.

a determinant role in their photocatalytic performance. To clarify this issue, we performed BET measurement for the three NB based samples, and found no significant difference in surface area among them. The result of BET measurement shows that the specific surface area of $Na_xH_{2-x}Ti_3O_7$ NBs was 32.5 m^2/g, comparable to 35.0 m^2/g of $H_2Ti_3O_7$ NBs. This result excludes the possible doubt that the observed superior photocatalytic performance of $Na_xH_{2-x}Ti_3O_7$ NBs originated from the difference of their surface area from the other samples. The surface area information further supports our demonstration that the intercalating Na atoms of $Na_xH_{2-x}Ti_3O_7$ NBs may effectively prohibit charge carriers from recombination, thus leading to the higher photocatalytic activity under UV illumination. On the other hand, as compared to the relevant commercial products like P-25 TiO_2 and $Na_2Ti_3O_7$ powders (Sigma–Aldrich, with the particle size of 0.1–1.0 μm), the as-synthesized $Na_xH_{2-x}Ti_3O_7$ NBs exhibited superior photocatalytic performance, attributable to the high crystallinity of NB structures that can facilitate the interior charge carrier transfer [57]. It is generally believed that structural defects in semiconductor would reduce the resulting photocatalytic activity since they could act as alternative sites for charge carrier recombination [57]. We thus suggested that the high crystallinity of $Na_xH_{2-x}Ti_3O_7$ NBs took major responsibility for their superior photocatalytic performance when compared with the commercial particulate powders, which were believed to have many structural defects like dislocations and grain boundaries. To further address this issue, we performed an acid-washing treatment on the commercial $Na_2Ti_3O_7$ powder and compared its photocatalytic performance. Upon the acid treatment in 0.1 M HCl solution for 72 h, $Na_2Ti_3O_7$ powder could be partially protonated to possess Na composition similar to $Na_xH_{2-x}Ti_3O_7$ NBs. The result of photocatalysis experiment shows that no evident improvement in the photocatalytic efficiency can be observed in HCl-treated $Na_2Ti_3O_7$ powder. This outcome confirms the beneficial effect of NB morphology on the photocatalytic performance of $Na_xH_{2-x}Ti_3O_7$. This demonstration can further emphasize the remarkable photocatalytic properties for the current $Na_xH_{2-x}Ti_3O_7$ NBs.

With the capability of effective light absorption in visible range, $Na_xH_{2-x}Ti_3O_7$ NBs might be promising as a visible-light-responsive photocatalyst. To investigate this potential, we further performed photocatalysis experiments under visible-light irradiation. Fig. 6c displays the results for the four Ti–O based samples used in the visible-light-driven TH photodegradation. Note that a small but not negligible activity was found for the calcinated $Na_xH_{2-x}Ti_3O_7$ and calcinated $H_2Ti_3O_7$ samples, which was mainly ascribed to the self-photosensitized effect [58] between dye molecules and the TiO_2 constituent. Of all the samples tested, only $Na_xH_{2-x}Ti_3O_7$ NBs showed satisfactory performance toward TH photodegradation after 180 min of irradiation. Since TH itself was not pyrolyzed in visible light, the vigorous activity of $Na_xH_{2-x}Ti_3O_7$ NBs observed here was entirely attributed to the outcome of photocatalysis using $Na_xH_{2-x}Ti_3O_7$. This demonstration reveals the potential as a highly efficient visible-light-driven photocatalyst for the current $Na_xH_{2-x}Ti_3O_7$ NBs.

3.5. *Effect of Au decoration*

With the decoration of Au nanoparticles, a further enhancement in the photocatalytic activity can be achieved for $Na_xH_{2-x}Ti_3O_7$ NBs. It should be mentioned that Au can serve as an efficient electron scavenger for $Na_xH_{2-x}Ti_3O_7$ due to its lower Fermi energetic level (+0.5 V versus NHE [59]) than the conduction band of $Na_xH_{2-x}Ti_3O_7$ (−0.3 V versus NHE, referring to the value reported for $H_2Ti_3O_7$ [52]). The photoexcited free electrons in $Na_xH_{2-x}Ti_3O_7$ NBs would thus preferentially transfer to the surface-decorated Au nanoparticles, simultaneously leaving photogenerated holes in NB domain to achieve charge separation. These separated charge carriers are highly reactive toward organic species, giving rise to a promising performance in the course of photocatalysis. Fig. 7a clearly illustrates the effect of Au decoration on the photocatalytic properties of $Na_xH_{2-x}Ti_3O_7$ NBs. With the decoration of Au of 0.5 and 1.0 wt%, the photocatalytic activity of $Na_xH_{2-x}Ti_3O_7$ NBs toward TH photodegradation increased correspondingly. This improvement mainly resulted from the deposited Au that can promote charge separation by attracting the photoexcited electrons from NBs, thus providing more electrons for the decomposition of TH. When the content of Au was increased from 1.0 to 3.0 wt%,

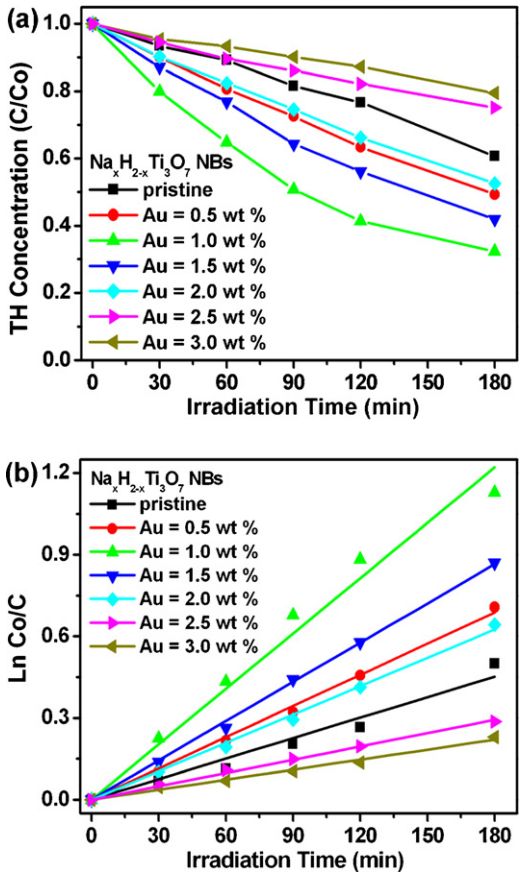

Fig. 7. TH photodegradation results under visible irradiation by using Au-decorated $Na_xH_{2-x}Ti_3O_7$ NBs with various Au contents. (a) C/C_o versus irradiation time plots, and (b) $\ln(C_o/C)$ versus irradiation time plots with the fitting results included.

a dramatic decrease in the photocatalytic activity was however observed. This phenomenon indicated that there is an optimal content of Au decoration for improving the photocatalytic performance of $Na_xH_{2-x}Ti_3O_7$ NBs. It has been widely documented that the excess content of metal may cover a large part of photocatalyst surfaces, which in turn decreases the number of active sites for photocatalysis as well as retards the access of light irradiation to photocatalyst surfaces [60]. Both of the above two circumstances may account for the depressed photocatalytic efficiency as observed here. Moreover, with increasing Au contents, electrons accumulated in Au became substantially abundant such that the photogenerated holes in NBs might be attracted and transferred to Au domain [61]. The electron–hole recombination would then be encouraged in Au, leading to the significant depletion of photoexcited charge carriers and thus the depression in photocatalytic efficiency. The photodegradation process can be further quantitatively interpreted through fitting to the pseudo-first-order reaction model, in which the apparent rate constant (k) of TH photodegradation can be determined according to the following expression [62]:

$$\ln\left(\frac{C}{C_o}\right) = -kt,$$

where C_o and C are the concentrations of TH at initial and at a certain irradiation time t, respectively, and k is equal to the slope of the fitting line.

Using the fitting results in Fig. 7b, we obtained the value of k as 0.0025, 0.0038, 0.0068, 0.0048, 0.0035, 0.0016, and 0.0012 min^{-1} for Au-decorated NBs with the Au content of 0, 0.5, 1.0, 1.5, 2.0, 2.5, and 3.0 wt%, respectively.

3.6. Effects of various metal decorations and recycling test

To demonstrate the remarkable photocatalytic properties for Au-decorated $Na_xH_{2-x}Ti_3O_7$ NBs, further comparative experiments were conducted. Four kinds of photocatalysts including Au-loaded, Au-decorated, Ag-decorated, and Pt-decorated $Na_xH_{2-x}Ti_3O_7$ NBs were used for TH photodegradation under the same experimental conditions. Note that Au-loaded NBs were prepared by simply mixing pristine $Na_xH_{2-x}Ti_3O_7$ NBs with Au colloids, resulting in a random distribution of Au nanoparticles around NBs. As to the fabrication of Ag- and Pt-decorated NB samples, a chemical reduction approach similar to that used in Au-decorated case was employed. The comparative results were shown in Fig. 8a, from which several points can be observed. First, Au-loaded $Na_xH_{2-x}Ti_3O_7$ NBs did not perform as better as Au-decorated NBs did, presumably owing to the less contact of Au with NBs in Au-loaded sample, which can be revealed from the corresponding TEM image shown in the inset of Fig. 8a. Because of the limited contact between Au and NBs, a retarded charge separation was expected for Au-loaded NB sample, thus leading to the lower photocatalytic efficiency. Similar result was ever reported for ZnS–Au composite system, in which the photocatalytic performance of Au-loaded ZnS was poorer than Au-decorated ZnS [63]. For the present Au-loaded NB sample, Au may still partly contact NB surfaces due to their random dispersion around NBs. This minor, but not insignificant, contact provided essential NB/Au interface for charge separation to proceed. Consequently, as compared to the pristine NBs, an evident enhancement in the resulting photocatalytic activity was still found in Au-loaded sample. It should be pointed out that the activity enhancement from Au-loaded NBs is not as pronounced as that from Au-decorated NBs, certainly because of the limited contact between Au and NBs in Au-loaded sample. This result reaffirms the notable charge separation which was believed to occur in the Au-decorated $Na_xH_{2-x}Ti_3O_7$ NBs and its benefit to the photocatalytic performance. Second, as compared to the Ag- and Pt-decorated samples, Au-decorated NBs exhibited superior photocatalytic efficiency toward TH photodegradation, which can be explained by the morphology divergence that existed among the deposited metals. As can be clearly seen in the insets of Fig. 8a, Ag and Pt grew as tinier particles (less than 5 nm in diameter) which covered much more densely on NB surfaces. The dependence of the size of metal on the photocatalytic performance of semiconductor has been investigated in Au/TiO_2 system [64]. Under a given loading amount of Au, Au/TiO_2 with reduced Au size showed depressed photocatalytic efficiency, which was attributed to the retarded charge separation resulting from the increasing number of Au on TiO_2. Since the much smaller size and the denser coverage of Ag and Pt in the present Ag- and Pt-decorated NBs were evident, we believed that an unfavorable effect, analogous to that of excess metal loading, would emerge to hinder the resulting photocatalytic performance. In addition to the size factor, the band structure [4,65] as well as the dye adsorption ability of metal might also affect the resulting photocatalytic performance of $Na_xH_{2-x}Ti_3O_7$ NBs. To investigate the recyclability and stability of these NBs, we performed a recycling test by using Au-decorated $Na_xH_{2-x}Ti_3O_7$ NBs with the Au content of 1.0 wt% as the representative photocatalyst. As shown in Fig. 8b, no appreciable decay of photocatalytic efficiency was found for Au-decorated NBs after they were repeatedly used and recycled in TH photodegradation for five times. Additionally, the morphology of these NBs remained unchanged after five cycles of photocatalysis, indicating that they did not suffer significant photocorrosion upon light irradiation. These results reveal that Au-decorated $Na_xH_{2-x}Ti_3O_7$ NBs could be promisingly utilized in the

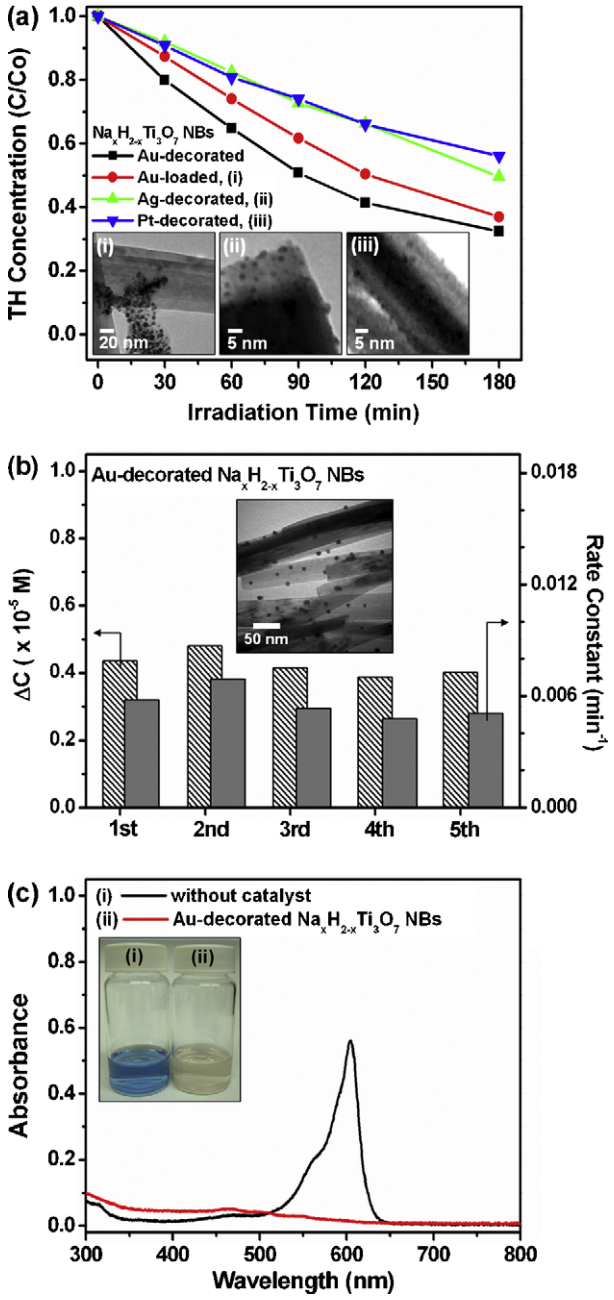

Fig. 8. (a) TH photodegradation results under visible-light irradiation by using different photocatalysts including Au-loaded, Au-decorated, Ag-decorated and Pt-decorated $Na_xH_{2-x}Ti_3O_7$ NBs. Content of metal = 1.0 wt%. The corresponding TEM images were shown in the inset. (b) Recycling test on Au-decorated $Na_xH_{2-x}Ti_3O_7$ NB photocatalyst under visible-light irradiation. Content of Au = 1.0 wt%. Inset shows the corresponding TEM image after they were used for five cycles of TH photodegradation. Duration of each cycle is 3 h. (c) Absorption spectra of TH solutions after exposure of 6 h of daytime sunlight without any catalyst and in the presence of Au-decorated $Na_xH_{2-x}Ti_3O_7$ NBs. Content of Au = 1.0 wt%. Insets show the corresponding solution color.

long-term course of photocatalysis. To further explore the applicability of these NBs in a more practical situation, their photocatalytic performance under natural sunlight was also evaluated. As illustrated in Fig. 8c, after exposure to 6 h of daytime sunlight, TH was totally degraded by using Au-decorated $Na_xH_{2-x}Ti_3O_7$ NBs, accompanied with an obvious decoloration of the resultant solution. This result shows that the current Au-decorated $Na_xH_{2-x}Ti_3O_7$ NBs can be used as highly efficient photocatalysts which may practically harvest energy from sunlight.

4. Conclusions

In conclusion, we have successfully synthesized Na-intercalated $H_2Ti_3O_7$ ($Na_xH_{2-x}Ti_3O_7$) NBs with an alkaline hydrothermal method and demonstrated for the first time that these NBs can effectively absorb visible light to carry out photocatalytic reactions. The intercalating Na atoms in $Na_xH_{2-x}Ti_3O_7$ NBs may invoke interband transition within their energy gap, thus resulting in the redshift of absorption band toward visible region. With the capability of effective light absorption in visible range, $Na_xH_{2-x}Ti_3O_7$ NBs performed much better in TH photodegradation than the other three counterpart products under visible-light irradiations. As compared to the relevant commercial products like P-25 TiO_2 and $Na_2Ti_3O_7$ powders, the as-synthesized $Na_xH_{2-x}Ti_3O_7$ NBs exhibited superior photocatalytic efficiency under UV illumination, attributable to the high crystallinity of NB structures that can facilitate the interior charge carrier transfer. A further enhancement in the photocatalytic activity can be achieved for $Na_xH_{2-x}Ti_3O_7$ NBs when Au nanoparticles of suitable amount were deposited on their surfaces. Due to the band offsets between $Na_xH_{2-x}Ti_3O_7$ and Au, a notable charge separation was expected to take place at the interface of $Na_xH_{2-x}Ti_3O_7$/Au, leading to the enhanced photocatalytic efficiency observed for Au-decorated $Na_xH_{2-x}Ti_3O_7$ NBs. The current Au-decorated $Na_xH_{2-x}Ti_3O_7$ NBs may find potential applications in relevant photocatalytic reactions such as water splitting and organics degradation. Moreover, Au-decorated $Na_xH_{2-x}Ti_3O_7$ NBs retained comparable photocatalytic activities after repeated uses and recycled, revealing that they could be promisingly utilized in the long-term course of photocatalysis. The present study gives rise to a new class of highly efficient hybrid photocatalysts that may practically harvest energy from sunlight.

Acknowledgements

This work was financially supported by the National Science Council of the Republic of China (Taiwan) under grants NSC-98-2113-M-009-015-MY2 and NSC-98-2218-E-009-003, and by National Chiao Tung University under grant 99W963.

References

[1] X. Hu, G. Li, J.C. Yu, Langmuir, in press. doi:10.1021/la902142b.
[2] S. Malato, P. Fernández-Ibáñez, M.I. Maldonado, J. Blanco, W. Gernjak, Catal. Today 147 (2009) 1–59.
[3] M. Jakob, H. Levanon, P.V. Kamat, Nano Lett. 3 (2003) 353–358.
[4] V. Subramanian, E.E. Wolf, P.V. Kamat, J. Am. Chem. Soc. 126 (2004) 4943–4950.
[5] T. Hirakawa, P.V. Kamat, J. Am. Chem. Soc. 127 (2005) 3928–3934.
[6] X.F. Wu, H.Y. Song, J.M. Yoon, Y.T. Yu, Y.F. Chen, Langmuir 25 (2009) 6438–6447.
[7] E. Elmalem, A.E. Saunders, R. Costi, A. Salant, U. Banin, Adv. Mater. 20 (2008) 4312–4317.
[8] R. Costi, A.E. Saunders, E. Elmalem, A. Salant, U. Banin, Nano Lett. 8 (2008) 637–641.
[9] H. Zeng, W. Cai, P. Liu, X. Xu, H. Zhou, C. Klingshirn, H. Kalt, ACS Nano 2 (2008) 1661–1670.
[10] J. Li, J. Xu, W.L. Dai, K. Fan, J. Phys. Chem. C 113 (2009) 8343–8349.
[11] N. Bao, L. Shen, T. Takata, K. Domen, Chem. Mater. 20 (2008) 110–117.
[12] Y. Li, Y. Hu, S. Peng, G. Lu, S. Li, J. Phys. Chem. C 113 (2009) 9352–9358.
[13] F.A. Frame, E.C. Carroll, D.S. Larsen, M. Sarahan, N.D. Browning, F.E. Osterloh, Chem. Commun. (2008) 2206–2208.
[14] C. Harris, P.V. Kamat, ACS Nano 3 (2009) 682–690.
[15] J.C. Yu, J. Yu, W. Ho, Z. Jiang, L. Zhang, Chem. Mater. 14 (2002) 3808–3816.
[16] W. Ho, J.C. Yu, S. Lee, Chem. Commun. (2006) 1115–1117.
[17] C. Yu, J.C. Yu, Catal. Lett. 129 (2009) 462–470.
[18] S.U.M. Khan, M. Al-shahry, W.B. Ingler Jr., Science 297 (2002) 2243–2245.
[19] D. Li, H. Haneda, S. Hishita, N. Ohashi, Chem. Mater. 17 (2005) 2596–2602.
[20] S. In, A. Orlov, F. García, M. Tikhov, D.S. Wright, R.M. Lambert, Chem. Commun. (2006) 4236–4238.
[21] P. Periyat, S.C. Pillai, D.E. McCormack, J. Colreavy, S.J. Hinder, J. Phys. Chem. C 112 (2008) 7644–7652.
[22] H. Irie, Y. Watanabe, K. Hashimoto, J. Phys. Chem. B 107 (2003) 5483–5486.
[23] Z.-G. Zhao, M. Miyauchi, Angew. Chem. Int. Ed. 47 (2008) 7051–7055.
[24] D.V. Bavykin, J.M. Friedrich, F.C. Walsh, Adv. Mater. 18 (2006) 2807–2824.

[25] V. Štengl, S. Bakardjieva, J. Šubrt, E. Večerníková, L. Szatmary, M. Klementová, V. Balek, Appl. Catal. B: Environ. 63 (2006) 20–30.
[26] C. Xing, D. Jing, M. Liu, L. Guo, Mater. Res. Bull. 44 (2009) 442–445.
[27] P. Umek, P. Cevc, A. Jesih, A. Gloter, C.P. Ewels, D. Arčon, Chem. Mater. 17 (2005) 5945–5950.
[28] A. Kleinhammes, G.W. Wanger, H. Kulkarni, Y. Jia, Q. Zhang, L.C. Qin, Y. Wu, Chem. Phys. Lett. 411 (2005) 81–85.
[29] D.V. Bavykin, A.A. Lapkin, P.K. Plucinski, J.M. Friedrich, F.C. Walsh, J. Phys. Chem. B 109 (2005) 19422–19427.
[30] S.H. Lim, J. Luo, Z. Zhong, W. Ji, J. Lin, Inorg. Chem. 44 (2005) 4124–4126.
[31] L. Kavan, M. Kalbáč, M. Zukalová, I. Exnar, V. Lorenzen, R. Nesper, M. Graetzel, Chem. Mater. 16 (2004) 477–485.
[32] J. Li, Z. Tang, Z. Zhang, Electrochem. Commun. 7 (2005) 62–67.
[33] S. Kubota, K. Johkura, K. Asanuma, Y. Okouchi, N. Ogiwara, K. Sasaki, J. Mater. Sci. Mater. Med. 15 (2004) 1031–1035.
[34] T. Kasuga, Thin Solid Films 496 (2006) 141–145.
[35] T. Kasuga, M. Hiramatsu, A. Hoson, T. Sekino, K. Niihara, Langmuir 14 (1998) 3160–3163.
[36] T. Kasuga, M. Hiramatsu, A. Hoson, T. Sekino, K. Niihara, Adv. Mater. 11 (1999) 1307–1311.
[37] D.L. Morgan, H.Y. Zhu, R.L. Frost, E.R. Waclawik, Chem. Mater. 20 (2008) 3800–3802.
[38] X. Sun, Y. Li, Chem. Eur. J. 9 (2003) 2229–2238.
[39] E. Morgado Jr., M.A.S. de Abreu, O.R.C. Pravia, B.A. Marinkovic, P.M. Jardim, F.C. Rizzo, A.S. Araújo, Solid State Sci. 8 (2006) 888–900.
[40] H.H. Ou, S.L. Lo, Y.H. Liou, Nanotechnology 18 (2007) 175702.
[41] H.H. Ou, C.H. Liao, Y.H. Liou, J.H. Hong, S.L. Lo, Environ. Sci. Technol. 42 (2008) 4507–4512.
[42] B. Lim, M. Jiang, J. Tao, P.H.C. Camargo, Y. Zhu, Y. Xia, Adv. Funct. Mater. 18 (2008) 1–12.
[43] R. Abe, M. Hara, J.N. Kondo, K. Domen, K. Shinohara, A. Tanaka, Chem. Mater. 10 (1998) 1647–1651.
[44] C.C. Chung, T.W. Chung, T.C.-K. Yang, Ind. Eng. Chem. Res. 47 (2008) 2301–2307.
[45] Y. Wang, G. Du, H. Liu, D. Liu, S. Qin, N. Wang, C. Hu, X. Tao, J. Jiao, J. Wang, Z.L. Wang, Adv. Funct. Mater. 18 (2008) 1131–1137.
[46] For bulk fcc Au, $d(1\,1\,1) = 0.2355$ nm from JCPDS 04-0784.
[47] P.J. Murphy, M.S. LaGrange, Geochim. Cosmochim. Acta 62 (1998) 3515–3526.
[48] P.J. Murphy, G. Stevens, M.S. LaGrange, Geochim. Cosmochim. Acta 64 (2000) 479–494.
[49] R. Zanella, S. Giorgio, C.R. Henry, C. Louis, J. Phys. Chem. B 106 (2002) 7634–7642.
[50] N. Wang, H. Lin, J. Li, X. Yang, B. Chi, C. Lin, J. Alloys Comp. 424 (2006) 311–314.
[51] L.M. Torres-Martìnez, I. Juárez-Ramírez, K.D. Ángel-Sánchez, L. Garza-Tovar, A. Cruz-López, G.D. Ángel, J. Sol-gel Sci. Technol. 47 (2008) 158–164.
[52] X.G. Xu, X. Ding, Q. Chen, L.-M. Peng, Phys. Rev. B 75 (2007) 035423.
[53] S. Eustics, M.A. El-Sayed, Chem. Soc. Rev. 35 (2006) 209–217.
[54] T. Hirakawa, P.V. Kamat, Langmuir 20 (2004) 5645–5647.
[55] L. Jing, H. Fu, B. Wang, D. Wang, B. Xin, S. Li, J. Sun, Appl. Catal. B: Environ. 62 (2006) 282–291.
[56] L.G. Devi, N. Kottam, S.G. Kumar, K.S.A. Raju, Catal. Lett. 131 (2009) 612–617.
[57] H.S. Jung, Y.J. Hong, Y. Li, J. Cho, Y. Kim, G. Yi, ACS Nano 2 (2008) 637–642.
[58] X. Yang, C. Cao, L. Erickson, K. Hohn, R. Maghirang, K. Klabunde, Appl. Catal. B: Environ. 91 (2009) 657–662.
[59] P.V. Kamat, B. Shanghavi, J. Phys. Chem. B 101 (1997) 7675–7679.
[60] I.M. Arabatzis, T. Stergiopoulos, D. Andreeva, S. Kitova, S.G. Neophytides, P. Falaras, J. Catal. 220 (2003) 127–135.
[61] W. Lu, S. Gao, J. Wang, J. Phys. Chem. C 112 (2008) 16792–16800.
[62] I.K. Konstantinou, T.A. Albanis, Appl. Catal. B: Environ. 49 (2004) 1–14.
[63] W.-T. Chen, Y.-J. Hsu, Langmuir 26 (2010) 5918–5925.
[64] T. Kiyonaga, M. Fujii, T. Akita, H. Kobayashi, H. Tada, Phys. Chem. Chem. Phys. 10 (2008) 6553–6561.
[65] H. Tada, F. Suzuki, S. Yoneda, S. Ito, H. Kobayashi, Phys. Chem. Chem. Phys. 3 (2001) 1376–1382.